Biomech Model Mechanobiol (2013) 12:763–780
DOI 10.1007/s10237-012-0440-5

ORIGINAL PAPER

A multiscale approach in the computational modeling of the biophysical environment in artificial cartilage tissue regeneration

Paola Causin · Riccardo Sacco · Maurizio Verri

Received: 15 February 2012 / Accepted: 30 August 2012 / Published online: 14 September 2012

Abstract Tissue Engineering is a strongly interdisciplinary scientific area aimed at understanding the principles of tissue growth to produce biologically functional replacements for clinical use. To achieve such an ambitious goal, complex biophysical phenomena must be understood in order to provide the appropriate environment to cells (nutrient delivery, fluid-mechanical loading and structural support) in the bioengineered device. Such a problem has an inherent multiphysics/multiscale nature, as it is characterized by material heterogeneities and interplaying processes occurring within a wide range of temporal and spatial scales. In this context, computational models are useful to gain a quantitative and comprehensive understanding of phenomena often difficult to be accessed experimentally. In this paper, we propose a mathematical and computational model that represents, to our knowledge, the first example of a self-consistent multiscale description of coupled nutrient mass transport, fluid-dynamics and biomass production in bioengineered constructs. We specifically focus on articular cartilage regeneration based on dynamically perfused bioreactors, and we investigate by numerical simulations three issues critical in this application. First, we study oxygen distribution in the construct, since achieving an optimal level throughout the construct is a main control variable to improve tissue quality. Second, we provide a quantitative evaluation of how interstitial perfusion can enhance nutrient delivery and, ultimately, biomass production, compared with static culture. Third, we perform a sensitivity analysis with respect to biophysical parameters related to matrix production, assessing their role in tissue regeneration.

Keywords Tissue Engineering · Multiscale model · Mass transfer in heterogeneous media · Model of biomass synthesis · Interstitial perfusion bioreactor

Abbreviations

TE	Tissue Engineering
ECM	Extracellular matrix
GAG	Glycosaminoglycan
CFD	Computational fluid-dynamics

1 Introduction

In vitro cultivation of functional tissues for body repair, the so-called "Tissue Engineering", is investigated as a promising technique able to improve life conditions of millions of patients worldwide (see, e.g., Langer and Vacanti 1993; Vunjak-Novakovic and Freshney 2006; Atala et al. 2011). Yet, at present, to bridge the gap between being a concept and a clinical applicable procedure, a definite need arises for improved control over the functional properties and composition of the cultivated tissue.

A major application of TE is found in the artificial regeneration of articular cartilage, a tissue with very poor capabilities of self repair. Portions of cartilage tissue have been grown in bioreactors starting from donor chondrocyte cells attached to polymeric scaffolds in mixed flasks, rotating wall or direct perfusion bioreactors (Freed and Vunjak-Novakovic 2001; Martin et al. 2004; Schulz and Bader 2007). Cells, initially

P. Causin (✉)
Dipartimento di Matematica "F. Enriques", Università degli Studi di Milano, via Saldini, 50, 20133 Milano, Italy
e-mail: paola.causin@unimi.it

R. Sacco · M. Verri
Dipartimento di Matematica "F. Brioschi", Politecnico di Milano, Piazza L. da Vinci, 32, 20133 Milano, Italy
e-mail: riccardo.sacco@polimi.it

M. Verri
e-mail: maurizio.verri@polimi.it

seeded so to yield a quasi-uniform thin layer on the scaffold walls (Wendt et al. 2006), undergo a first period of rapid proliferation during the early culture time (5–7 days), after which they secrete (2–4 weeks) the typical highly hydrated matrix comprising proteoglycan monomers assembled with GAGs anchored to hyaluronic acid chains and collagen (Potter et al. 1998; Freed and Vunjak-Novakovic 2001). In order to ensure cell viability and efficient metabolic activity, a properly tuned level of nutrients must be delivered to cells. This is not an easy task, since nutrient mass transfer is significantly limited by the progressive obstruction of the scaffold due to biomass growth (Obradovic et al. 1999; Freed and Vunjak-Novakovic 2001). Direct perfusion bioreactors have been shown to be able to deliver more efficiently nutrient to cells, and for this reason, they are the reference devices in this work. The specific experimental setting we consider (described in detail in Raimondi et al. 2006, 2008) consists of scaffolds with average porosity 77 %, interstitially perfused by the culture medium through a pumping system. The medium flow rate at the inlet is kept constant all over the experiment, and the flow direction is inverted cyclically every 40 min. The presence of an interstitial flow has the side effect of introducing further mechanical and biophysical processes which must be as well analyzed and controlled.

The biophysical phenomena occurring during in vitro tissue regeneration encompass a wide range of embedded scales, as depicted in Fig. 1. Existing mathematical models mainly focus on a single specific scale. Computational models working at the *Macroscale* treat the perfused scaffold as a continuum on which the Bioengineer defines and modifies the control parameters (inlet velocity, scaffold porosity). These studies numerically evaluate the fluid-dynamical field and/or the nutrient profile in the construct as if the system were simply a "homogeneous equivalent fluid" (Obradovic et al. 1999, 2000; Devarapalli et al. 2009; Williams et al. 2002). Deposition of biomass is controlled via phenomenological models keeping into account the dependence of growth on local nutrient availability and, in a simplified manner, of mutual inhibition effects (Nikolaev et al. 2010). CFD models of interstitially perfused bioreactors coupled with oxygen mass transport equations are treated in Raimondi et al. (2006, 2012), Raimondi (2006) and are localized in microdomains composed of a few pores (functional units), corresponding to the *Mesoscale*. The problem is solved on idealized simplified geometries as well as on realistic configurations, keeping into account the presence of the scaffold matrix. The CFD analysis is, however, carried out on the uncellularized scaffold, that is, completely neglecting the presence of the growing biomass. An improvement is obtained in Lesman et al. (2010) where CFD computations are performed on a series of different "frozen" simplified geometries representing the pattern of deposition of the biomass extracted from experimental images at the pore size for different time levels. In Galbusera et al. (2007), the computational study is carried out at the *Microscale*, and the CFD analysis/mass transport is coupled with a representation of the *Cellular scale* based on the use of cellular automata algorithms including in a simplified manner phenomena like adhesion and contact forces.

Adopting a single-scale perspective as the one of the above models can provide useful insights on selected phenomena in the bioreactor. However, a change of perspective is strongly needed to improve the TE practice: this corresponds to maintain a Macroscale vision, which is the one important for the Bioengineer, including at the same time a powerful lens to model finer scale (*Microscale*) effects. At present, however, only a very restricted selection of models is capable of treating multiple scales in this context, since this requires to address the very delicate concept of scale transition in a very complex framework. In Cioffi et al. (2008), a first attempt was carried out, by solving an axial symmetric model at the Macroscale to compute boundary conditions that are then used to drive the solution of a 3D CFD model in a Microscale domain constituted by the uncellularized scaffold geometry. In this reference, no feedback mechanism was introduced between the Microscale and Macroscale models. An alternative way to include, in a coupled fashion, information coming from finer scales into larger scale models is to resort to homogenized approaches characterized by effective transport parameters computed from (complex) closure problems localized at the Microscale (Whitaker 1999). In Chung et al. (2007), such an approach was applied to a Darcy model for the porous medium coupled with convection diffusion equations for nutrient mass transport in combination with cell growth models derived from the works of Galban and Locke (1999a,b). In our previous paper Sacco et al. (2011), the same approach as in Chung et al. (2007) is considered with the further use of suitably extended analytical solutions for the closure problems accounting for the presence of the scaffold. In the present article, we adopt the homogenized perspective of Sacco et al. (2011), at the same time including, in the spirit of Cioffi et al. (2008), a Microscale analysis which impacts on the Macroscale study via a genuinely dynamically coupled mechanism. The present modeling strategy is characterized by:

- a self-consistent coupling among nutrient distribution, cell metabolic activity and geometry evolution;
- a biophysical description of biomass evolution;
- a subdivision into modular sub-blocks, whose modeling/computational complexity can be properly tuned to the problem at hand without affecting the overall structure;
- an affordable computational cost;
- the possibility of a direct integration with experimental data obtained from microscopical images of histological sections of tissue-engineered constructs.

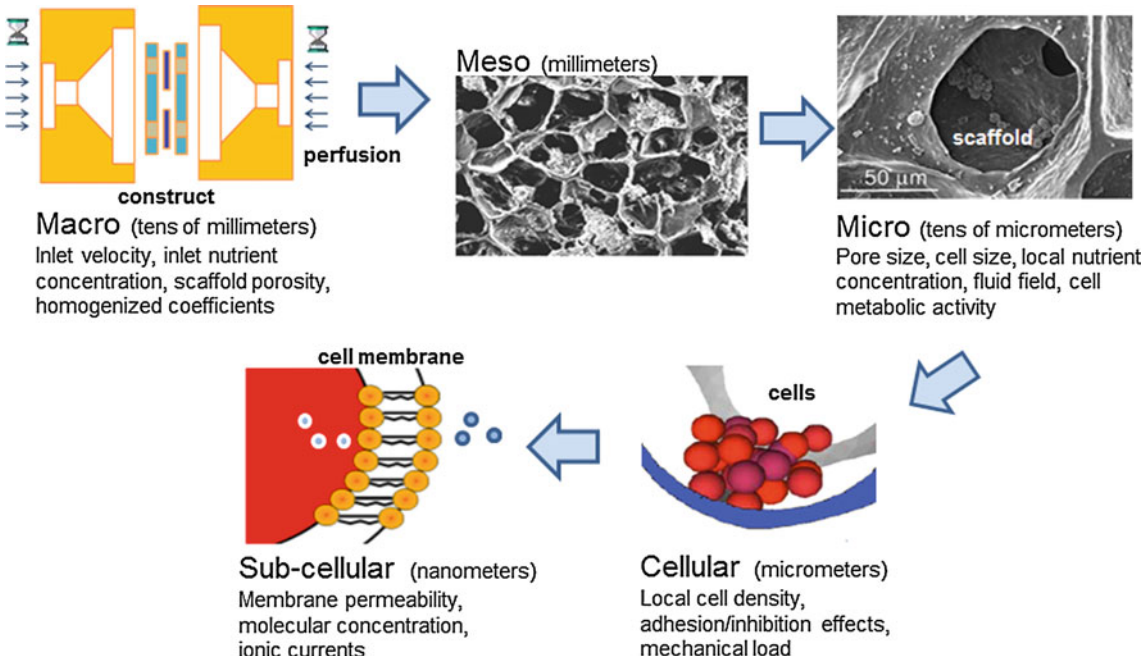

Fig. 1 The TE problem is characterized by the presence of complex phenomena occurring at different scales. The figure depicts such situation in a schematism useful for the mathematical modelization

We use such a multiscale computational framework to carry out three distinct studies addressing important issues in cartilage regeneration. The first study stems from the observation that cartilage cells are in vivo physiologically subjected to low levels of oxygen tension (p_{O_2} ranging from 2 to 10 %), but a widespread practice in TE is to supply "hyperphysiological" conditions ($p_{O_2} = 20\,\%$) at the bioreactor inlet (Grimshaw and Mason 2001; Das et al. 2010). We carry out simulations to relate a given inlet nutrient concentration with the time evolution of the corresponding distribution inside the construct, and we explore how inlet concentration can be tuned to optimize local oxygenation levels. In a second study, we investigate the effect of perfusion on nutrient mass transfer. Perfusion, enhancing nutrient delivery, allows for a more uniform development of biomass across the construct thickness, requiring a shorter culture time to reach a certain biomass production level with respect to the static case. The better performance of dynamical perfusion compared to static culture is confirmed by our simulations, which show, however, that, while the transient behavior to reach steady state is significantly different from static culture conditions, the final level of oxygen obtained in dynamical conditions is definitely influenced by diffusion barriers. Eventually, in a third study, we further assess the role of diffusion barriers, carrying out a sensitivity analysis on the biomass production rate and extracellular matrix inhibition effect with respect to biomass growth.

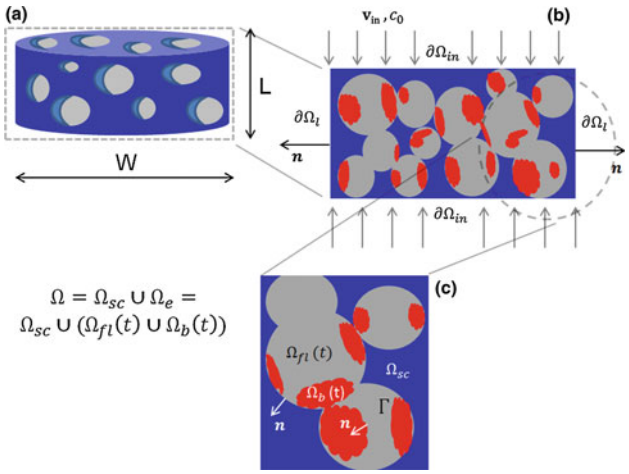

Fig. 2 Geometry and notation. **a** 3D porous construct. **b** 2D cross-section of the construct, with length L and thickness W. **c** Zoomed view of the multiphase composition of the construct

2 Mathematical model

We consider the typical configuration of a disk-shaped scaffold consisting of the union of interconnected scaffold pores, culture medium and biomass. We let $\mathbf{x}$ be the coordinate vector, t the time variable and $I_t := [t_{\text{start}}, t_{\text{end}}]$ the temporal interval of engineered tissue cultivation, t_{start} and t_{end} being the starting and final culture times. Figure 2 shows the construct geometry and introduces the corresponding notation

used throughout the paper. We denote by Ω the bioreactor domain, with boundary $\partial\Omega = \partial\Omega_{\text{in}} \cup \partial\Omega_l$. The domain Ω is composed by the time-invariant subdomain Ω_{sc}, representing the scaffold, and by its complement $\Omega_e = \Omega_e(t)$. This latter subdomain is, in turn, composed of the time-dependent fluid portion $\Omega_{\text{fl}} = \Omega_{\text{fl}}(t)$ and the biomass portion $\Omega_{\text{b}} = \Omega_{\text{b}}(t)$, both of which may be, in general, composed by the union of unconnected domains of complex shape. The interface separating Ω_{fl} and Ω_{b} is denoted by Γ. Moreover, $\mathbf{n}$ indicates the unit normal vector on $\partial\Omega$ and on each material interface.

2.1 Full scale model

The full scale approach we advocate in this work consists of the coupled solution for every $t \in I_t$ of the following differential systems.

2.1.1 Fluid subdomain model

(a) advection–diffusion problem for nutrient concentration $c = c(\mathbf{x}, t)$ in Ω_{fl}:

$$\frac{\partial c}{\partial t} + \nabla \cdot \mathbf{J} = 0, \tag{1a}$$

$$\mathbf{J} = -D_{\text{fl}} \nabla c + \mathbf{v}c, \tag{1b}$$

where $\mathbf{v}$ is the fluid velocity determined by system (2), $\mathbf{J}$ is the nutrient mass flux and D_{fl} is the nutrient diffusivity in the fluid phase. The equation system (1) is supplied with the initial condition $c(\mathbf{x}, 0) = c_0$ and the boundary conditions $c = c_0$ on $\partial\Omega_{\text{fl}} \cap \partial\Omega_{\text{in}}$ and $\mathbf{J} \cdot \mathbf{n} = 0$ on $\partial\Omega_{\text{fl}} \cap \partial\Omega_l$ and on $\partial\Omega_{\text{fl}} \cap \partial\Omega_{\text{sc}}$, where c_0 is the (constant) inlet nutrient concentration.

(b) Navier–Stokes equations (Landau and Lifshtiz 1959) for fluid velocity $\mathbf{v} = \mathbf{v}(\mathbf{x}, t)$ and fluid pressure $p = p(\mathbf{x}, t)$ in Ω_{fl}:

$$\nabla \cdot \mathbf{v} = 0, \tag{2a}$$

$$\rho_{\text{fl}} \left[\frac{\partial \mathbf{v}}{\partial t} + (\mathbf{v} \cdot \nabla)\mathbf{v} \right] = -\nabla p + \mu_{\text{fl}} \triangle \mathbf{v}, \tag{2b}$$

where ρ_{fl} and μ_{fl} are the density and the dynamic viscosity of the medium, respectively. The equation system (2) is supplied with the initial condition $\mathbf{v}(\mathbf{x}, 0) = \mathbf{0}$ and the boundary conditions $\mathbf{v} = \mathbf{v}_{\text{in}}$ on $\partial\Omega_{\text{fl}} \cap \partial\Omega_{\text{in}}$, $\mathbf{v} = \mathbf{0}$ on $\partial\Omega_{\text{fl}} \cap \partial\Omega_{\text{sc}}$, and $\partial\mathbf{v}/\partial\mathbf{n} = \mathbf{0}$ on $\partial\Omega_{\text{fl}} \cap \partial\Omega_l$.

2.1.2 Biomass subdomain model

(a) diffusion–reaction problem for nutrient concentration $c = c(\mathbf{x}, t)$ in Ω_{b}:

$$\frac{\partial c}{\partial t} + \nabla \cdot \mathbf{J} = Q \tag{3a}$$

$$\mathbf{J} = -D_{\text{b}} \nabla c, \tag{3b}$$

where D_{b} is the nutrient diffusivity in the biomass phase and the function $Q = Q(c)$ represents mass consumption due to cellular metabolism, expressed by the Michaelis–Menten kinetics

$$Q = -\frac{R\,c}{K_{1/2} + c}, \tag{3c}$$

where $R = \Psi_{\max} \xi_{\text{cells}}$, ξ_{cells} being the number of cells per unit biomass volume and $\Psi_{\max}$ the maximal nutrient consumption rate, respectively, while $K_{1/2}$ is the half saturation constant. The equation system (3) is supplied with the initial condition $c(\mathbf{x}, 0) = c_0$ and the boundary conditions $c = c_0$ on $\partial\Omega_{\text{b}} \cap \partial\Omega_{\text{in}}$ and $\mathbf{J} \cdot \mathbf{n} = 0$ on $\partial\Omega_{\text{b}} \cap \partial\Omega_l$ and on $\partial\Omega_{\text{b}} \cap \partial\Omega_{\text{sc}}$;

(b) model for fluid velocity in Ω_{b}:

$$\mathbf{v} = \mathbf{0}; \tag{4}$$

(c) model for biomass growth:

$$\Omega_{\text{b}} = \Omega_{\text{b}}(t; \mathbf{v}|_{\partial\Omega_{\text{fl}} \cap \partial\Omega_{\text{b}}}, p_1, \ldots, p_n), \tag{5}$$

where $(p_1, \ldots, p_n)$ is a set of biophysical parameters (e.g., nutrient concentration, contact inhibition effects) that regulate engineered tissue production at the Microscale level.

2.1.3 Fluid–biomass interface model

At the fluid–biomass interface, the following conditions must be satisfied:

$$c|_{\partial\Omega_{\text{b}}} = \kappa c|_{\partial\Omega_{\text{fl}}}, \tag{6a}$$

$$\mathbf{J}|_{\partial\Omega_{\text{fl}}} \cdot \mathbf{n} = \mathbf{J}|_{\partial\Omega_{\text{b}}} \cdot \mathbf{n}, \tag{6b}$$

$$\mathbf{v}|_{\partial\Omega_{\text{fl}}} = \mathbf{0}. \tag{6c}$$

Condition (6a) expresses local mass equilibrium, with positive constant $\kappa \leq 1$, and provides a "lumped" description of the effects of transmembrane chemical processes occurring at the subcellular scale (Wood et al. 2002). Condition (6b) represents mass flux continuity, while condition (6c) is the standard adherence of a fluid at a solid wall. We will refer in the following to the above coupled system of equations as the 3D Full Scale (3DFS) model.

2.1.4 Modeling assumptions

The following assumptions in the mathematical description of engineered tissue growth will be adopted in the present work.

A1. Nutrient mass transfer can be described by a sequence of quasi-stationary steps, because the time scale of nutrient transport is much faster than biomass growth (Obradovic et al. 2000; Sacco et al. 2011). This corresponds to neglecting the term $\partial c/\partial t$ in (1a) and (3a). Notice that the temporal dependence of the fields c and $\mathbf{v}$ is, however, retained through the coupling with biomass growth.

A2. The left-hand side of (2b) can be neglected because the Reynolds number of the fluid-dynamical problem is very small. For example, assuming an inlet velocity $|\mathbf{v}_{\text{in}}| = 50\,\mu\text{ms}^{-1}$, a scaffold porosity of 77 % (Raimondi et al. 2005) and $L = 1\,\text{mm}$ (Sacco et al. 2011), we have that the microscopic Reynolds number (i.e., computed at the pore size scale) is of the order of 5×10^{-4}, while the macroscopic Reynolds number (i.e., computed at bioreactor scale) is of the order of 6×10^{-2}.

A3. Biomass growth is described according to the fact that, after seeding, cells undergo a first proliferative phase, followed by an intense phase of ECM secretion. Since proliferation is a time-limited but highly complex mechanism, whose modeling is a very hard task which should be addressed as a stand-alone topic, we introduce in this work the approximation of a "post-initial" condition, which amounts to assuming that cells have already reached their maximal number $N^{\text{tot}}_{\text{cells}}$ (see Obradovic et al. 2000; Nikolaev et al. 2010 for a similar approach). Moreover, we consider cells and biomass to have the same mass density ρ_{b}, which will be assumed to be equal to the clear fluid density ρ_{fl}.

Depending on the choice of initial conditions, we notice that assumptions A1. and A2. might fail to hold in a short temporal interval immediately after the starting culture time $t = t_0$, during which transient and inertial effects might play a significant role.

2.1.5 Idealized geometry

A realistic geometry of the construct can be extracted from μ-CT data and used, upon segmentation and post-processing, for simulations. Since this is not the focus of this work, we rather consider the idealized geometry shown in Fig. 3a, referred to the experimental setting of Raimondi et al. (2008) and already numerically investigated by several authors (Raimondi et al. 2005; Cioffi et al. 2008; Lesman et al. 2010). The simplified bioreactor domain is described by a regular mosaic of "cubic pores" (Fig. 3a, b), obtained by intersecting a cube of size $2b$ with a sphere of radius R_{sph}, such that $b < R_{\text{sph}} < b\sqrt{2}$. We denote by $2a$ the diameter of the circle obtained on the lateral sides of the cube from the intersection

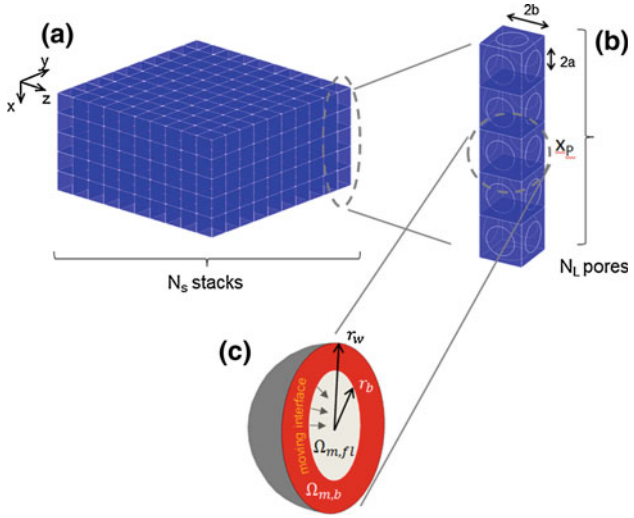

Fig. 3 Idealized geometry. **a** The bioreactor construct is composed by a regular mosaic of "cubic pores" which represent the functional sub–units. The cubic pores are organized in N_S stacks. **b** Stack of pores. Each stack is partitioned into N_L pores and is aligned along the x axis, along which the coordinate of the centroid of the pore P is denoted by x_P. **c** Spherical pore. The origin of the coordinate system is located at the pore center, the fluid–biomass interface at $r_{\text{b}} = r_{\text{b}}(t)$ and the pore wall at $r = r_{\text{w}}$, respectively. Biomass is supposed to uniformly grow inwardly along the radial direction

with the sphere. Letting then $V_{\text{cub}} = (2b)^3$ the volume of the cube, we define the construct design porosity Φ_0 as

$$\Phi_0 := \frac{V^0_{\text{void}}}{V_{\text{cub}}} = \frac{4\pi R^3_{\text{sph}}/3 - 6\pi h^2(3R_{\text{sph}} - h)/3}{8b^3} = \frac{\pi}{24}(-8\lambda^3 + 18\lambda^2 - 6)$$

where V^0_{void} is the void volume in the cube at the starting culture time, $h := R_{\text{sph}} - b$ and $\lambda := R_{\text{sph}}/b$, with $1 < \lambda < \sqrt{2}$. During the temporal evolution of the engineered tissue growth process, ECM production progressively tends to fill the available void space within each pore of the scaffold matrix, so that permeability to fluid flow and diffusivity of nutrient delivery are expected to be considerably reduced. This effect is accounted for by our multiscale model through the introduction of suitable *effective transport parameters* (effective permeability, effective diffusivity) discussed in Sect. 2.3.

2.2 Multiscale model

Even with the introduction of the above simplifications, the computational challenge of solving the 3DFS model is still a too demanding task even for the more advanced numerical techniques and powerful machine resources. This difficulty is principally represented by the need of using a very high scale resolution, say, up to the Microscale/Cellular scale, further complicated by the presence of internal moving boundaries due to biomass growth. A change of modeling perspective is

thus required. The idea we pursue in this work is to use a scale separation argument and localize the 3DFS model at two distinct—but interacting—scales, the Macro- and Micro-scales. At the Macroscale level, a homogenized form of the 3DFS model is used for the gross characterization of internal fields and inclusion of technological input parameters, while at the Microscale level, a decoupled solution of the 3DFS model is carried out on disjoint computational domains of strongly reduced size for the characterization of fine biomass growth phenomena and direct interaction with high-resolution experimental measurements. The two scales are coupled and interact through bridging variables, which for Micro-to-Macro transition represent effective-averaged parameters, while for Macro-to-Micro transition represent appropriate boundary conditions.

To mathematically identify in the rest of the paper each of the two scale levels introduced above, we will denote by the subscripts m and M quantities and operators defined at the Microscale and Macroscale, and by (m,M) and (M,m) quantities obtained from Micro-to-Macro- and Macro-to-Micro-scale transitions, as described below.

2.2.1 The Microscale model

The Microscale model is formulated at a characteristic size corresponding to the functional sub-unit constituted by the single pore. Despite the strong size reduction with respect to the 3DFS problem, the difficulty of computationally handling moving interfaces in a 3D domain remains unsolved. A possible escape to this difficulty relies on the experimental evidence that biomass growth mainly occurs in the void spherical space symmetrically along the pore radial direction (Lesman et al. 2010). This suggests, providing at the same time a biophysical justification, to introduce in the mathematical description of Microscale phenomena the assumption of *spherical symmetry*. With this assumption, the intrinsic 3D nature of the biomass growth is maintained at the benefit of a drastic reduction of computational complexity because all problem variables depend only on the radial coordinate. To work under this hypothesis, we introduce an "equivalent spherical pore" (Fig. 3c) consisting of a sphere of radius r_w whose volume $V_\mathrm{w} = 4\pi r_\mathrm{w}^3/3$ is equal to the void volume of the pore, which yields $r_\mathrm{w} = b(6\Phi_0/\pi)^{1/3}$. The spherical pore is adopted as the computational domain Ω_m and is composed of the union of the time-varying fluid and biomass micro-regions $\Omega_{\mathrm{m,fl}}$ and $\Omega_{\mathrm{m,b}}$ (Fig. 3c). The origin of the radial system is located at the centroid $\mathbf{x}_P$ of the considered pore P. To simplify the notation, the dependence on $\mathbf{x}_P$ of all the quantities in the Microscale model will be understood, if not otherwise specified.

The 3DFS model localized at the Microscale level amounts to solving the following coupled differential sub-systems for every $t \in I_t$:

(a) model for Microscale nutrient concentration $c_\mathrm{m} = c_\mathrm{m}(r,t)$:

(1) in the Microscale fluid subdomain $\Omega_{\mathrm{m,fl}}$:

$$c_\mathrm{m} = c_{(\mathrm{M,m})}, \tag{7}$$

where $c_{(\mathrm{M,m})}$ is the Macro- to Micro-scale bridging concentration;

(2) in the Microscale biomass subdomain $\Omega_{\mathrm{m,b}}$:

$$\frac{1}{r^2}\frac{\partial (r^2 J_\mathrm{m}(c_\mathrm{m}))}{\partial r} = Q(c_\mathrm{m}), \tag{8a}$$

$$J_\mathrm{m}(c_\mathrm{m}) = -D_\mathrm{b}\frac{\partial c_\mathrm{m}}{\partial r}. \tag{8b}$$

The equation system (8) is supplied with the following interface and boundary conditions:

$$c_\mathrm{m} = \kappa c_{(\mathrm{M,m})} \quad \text{at} \quad r = r_\mathrm{b}, \tag{8c}$$

$$J_\mathrm{m}(c_\mathrm{m}) = 0 \quad \text{at} \quad r = r_\mathrm{w}, \tag{8d}$$

where a remark similar to that made for condition (6a) applies also to the interface condition (8c);

(b) model for the radial component of the Microscale fluid velocity $v_\mathrm{m} = v_\mathrm{m}(r,t)$:

(1) in the Microscale fluid subdomain $\Omega_{\mathrm{m,fl}}$:

$$v_\mathrm{m} = \alpha/r^2, \tag{9a}$$

where $\alpha = \alpha(t)$ is a function to be determined enforcing the continuity of convective (from the left) and diffusive (from the right) nutrient fluxes at $r = r_\mathrm{b}$, that is

$$\frac{\alpha}{r_\mathrm{b}^2} c_{(\mathrm{M,m})} = J_\mathrm{m}(c_\mathrm{m})\big|_{r\downarrow r_\mathrm{b}}, \tag{9b}$$

where $(\cdot)\big|_{r\downarrow r_\mathrm{b}} := \lim_{\varepsilon_r \to 0^+} (\cdot)\big|_{r_\mathrm{b}+\varepsilon_r}$. Notice that the singularity of v_m at $r = 0$ has no physical significance; rather, it is a mathematical consequence of the fact that Eq. (9a) is the only admissible spherically symmetric solution of the Stokes equation.

(2) in the Microscale biomass subdomain $\Omega_{\mathrm{m,b}}$:

$$v_\mathrm{m} = 0. \tag{9c}$$

The above simplified mathematical representation of fluid flow is in accordance with the 2D and 3D simulation experiments conducted in Raimondi et al. (2011) on the novel mini-bioreactor configuration experimentally studied in Laganà and Raimondi (2011) and corresponds to assuming that nutrient delivery throughout growing biomass is to be ascribed principally to the mechanism of oxygen diffusion.

(c) model for biomass radial thickness and interface displacement:
secretion of biomass from cells causes the medium-biomass interface to move due to the increase in the width of the region $\Omega_{\mathrm{m,b}}$ at the expense of a reduction of $\Omega_{\mathrm{m,fl}}$. In radial symmetry, the biomass region is identified by the evolution of the quantity $h_{\mathrm{b}} := r_{\mathrm{w}} - r_{\mathrm{b}}$, which represents the time-dependent thickness of the biomass and consists of cells and accumulated extracellular matrix.
Before describing the model in detail, we need to establish some notation and fundamental relationships. Let $V_{\mathrm{b}} = V_{\mathrm{b}}(t) = V_{\mathrm{w}} - 4\pi(r_{\mathrm{w}} - h_{\mathrm{b}}(t))^3/3$ denote the volume occupied by the biomass in the spherical pore at time t. Then, the amount of biomass present at time t in pore P is $m_{\mathrm{b}}(t) = \rho_{\mathrm{b}} V_{\mathrm{b}}(t)$. We assume the biomass at time $t = 0$ to be purely composed of a layer of $N^{\mathrm{tot}}_{\mathrm{cells}}$ cells—which according to the previous assumption on the "post-initial" condition is a fixed given value—forming an equivalent annular region of thickness h_0, so that $m_{\mathrm{b}}(0) = \rho_{\mathrm{b}}(V_{\mathrm{w}} - 4\pi(r_{\mathrm{w}} - h_0)^3/3)$.
To monitor biomass secretion, we follow the standard experimental and theoretical practice of choosing GAG as a marker of ECM accumulation. For modeling simplicity, we focus only on the evolution of the GAG "bound" fraction (see also Wilson et al. 2002); we refer to DiMicco and Sah (2003), Klein and Sah (2007) for a more general and detailed description including unbound, bound and degraded GAG fractions. Denoting by $m_{\mathrm{GAG}} = m_{\mathrm{GAG}}(t)$ the GAG mass contained at time t in $\Omega_{\mathrm{m,b}}$, we assume the following 0D lumped model of the GAG synthesis process (Obradovic et al. 2000; Nikolaev et al. 2010):

$$\frac{\mathrm{d}m_{\mathrm{GAG}}}{\mathrm{d}t} = k_{\mathrm{GAG}}\,\xi_{\mathrm{cells}}\,\bar{c}_{\mathrm{m}}\left(1 - \frac{m_{\mathrm{GAG}}}{m_{\mathrm{GAG,inh}}}\right) \tag{10a}$$

$$m_{\mathrm{GAG}}(0) = 0, \tag{10b}$$

where k_{GAG} is the GAG synthesis rate, $\xi_{\mathrm{cells}}(t) = N^{\mathrm{tot}}_{\mathrm{cells}}/V_{\mathrm{b}}(t)$ the time-dependent volumetric density of cells secreting biomass, and $\bar{c}_{\mathrm{m}} = \bar{c}_{\mathrm{m}}(t)$ the average Microscale nutrient concentration in the biomass. Product inhibition is taken into account by including in the right-hand side of (10a) the dependence on a saturation GAG level $m_{\mathrm{GAG,inh}}$. This term represents in a simplified way the inhibitory feedback effect exerted by cell surface hyaluronan receptors and integrins in the assembly of the matrix, which "sense" the location and quantity of GAG and collagen and send messages to maintain homeostatic concentrations (Knudson and Knudson 1991). To close the problem, we need to connect the GAG mass production to the whole biomass amount. With this aim, we assume the following constitutive relation

$$m_{\mathrm{b}}(t) = m_{\mathrm{b}}(0) + E\,m_{\mathrm{GAG}}(t), \tag{11}$$

where the parameter $E > 1$ keeps into account the fact that the natural cartilagineous ECM is composed for the 70–80 % of its wet weight of water, while in the remaining fraction of the wet weight, the 10–15 % are collagen fibrils and the 5 % are GAG components, respectively (Buschmann et al. 1992). Introducing for brevity the auxiliary variable $y(t) := 1 - h_{\mathrm{b}}(t)/r_{\mathrm{w}}$, representing the normalized radius of the fluid domain, so that $y(0) = 1 - h_0/r_{\mathrm{w}}$, the following functional relation between the biomass thickness and the secreted GAG mass holds

$$y(t) = y(0)\sqrt[3]{1 - \frac{E\,m_{\mathrm{GAG}}(t)}{\rho_{\mathrm{b}} V_{\mathrm{w}}(y(0))^3}}, \tag{12}$$

where $m_{\mathrm{GAG}}(t)$, in practical computations, will be the result of an appropriate numerical approximation of problem (10). Since $y(t)$ must be a non-negative quantity, we immediately get the following constraint on the GAG mass that can be accumulated at each time level $t \geq 0$ due to sole geometrical restrictions

$$0 \leq m_{\mathrm{GAG}}(t) \leq \frac{\rho_{\mathrm{b}} V_{\mathrm{w}}}{E}(y(0))^3 := m_{\mathrm{GAG}^*}.$$

At the same time, contact inhibition effects included in model (10) imply that

$$m_{\mathrm{GAG}}(t) \leq m_{\mathrm{GAG,inh}} \quad \forall t \geq 0.$$

Combining the two bounds, we obtain that the maximum theoretical value of the biomass thickness, denoted by $h_{\mathrm{b,max}}$, is given by

$$h_{\mathrm{b,max}} = r_{\mathrm{w}} \min\left\{\left(1,\, 1 - y(0)\sqrt[3]{1 - \frac{m_{\mathrm{GAG,inh}}}{m_{\mathrm{GAG}^*}}}\right)\right\}. \tag{13}$$

2.2.2 *The Macroscale model*

The Macroscale problem is formulated in the idealized bioreactor domain $\Omega_{\mathrm{M}} \equiv \Omega$ shown in Fig. 3a. The main modeling assumption to reduce the complexity of the 3DFS model is to consider a homogenized continuum version of the corresponding equations, that is uniformly valid in the whole domain Ω_{M}. To further reduce the computational cost, we also assume that nutrient mass transport across neighboring pores in the (y, z) plane can be neglected and that boundary

effects on the lateral walls of the construct can be ignored as well. Let us denote by $\mathcal{P}_H$ the collection of N_L cubic pores P of size $2b$ that constitute an ordered stack composing Ω_{M}: due to the above hypothesis, the stack is a 1D (x-dependent) domain, over which solutions requiring a low computational effort will be sought. Moreover, even if each stack has in principle its own dynamics, in the present device configuration, it is reasonable to assume that all the pores located in the same (y, z) plane are indistinguishable, that is, they are supplied with the same amount of nutrient and they exhibit the same cellular metabolic activity, so that they have the same bio-physical behavior. The global bioreactor behavior is thus the overall contribution of the parallel of the N_S indistinguishable stacks. All the above hypotheses are supported by our computational experience with multi-dimensional simulations (Sacco et al. 2011; Raimondi et al. 2012) and by several other simulations reported in the literature (see, e.g., Cioffi et al. 2008).

The 3DFS model localized at the Macroscale level amounts to solving in Ω_{M} the following coupled differential sub-systems for every $t \in I_t$:

a) model for nutrient concentration $c_{\mathrm{M}} = c_{\mathrm{M}}(x, t)$:

$$\frac{\partial J_{\mathrm{M}}(c_{\mathrm{M}})}{\partial x} = Q_{\mathrm{M}}(c_{\mathrm{M}}), \tag{14a}$$

$$J_{\mathrm{M}}(c_{\mathrm{M}}) = -D_{(\mathrm{m,M})}\frac{\partial c_{\mathrm{M}}}{\partial x} + v_{\mathrm{M}}\, c_{\mathrm{M}}, \tag{14b}$$

where v_{M} is the Macroscale velocity field determined from system (15) and

$$Q_{\mathrm{M}}(c_{\mathrm{M}}) = \frac{R_{(\mathrm{m,M})}\, c_{\mathrm{M}}}{K_{1/2} + c_{\mathrm{M}}}.$$

The coefficients $D_{(\mathrm{m,M})}$ and $R_{(\mathrm{m,M})}$ are the *effective* nutrient diffusivity and consumption rate, respectively, computed as described in Sect. 2.3. The equation system (14) is supplied by the boundary conditions $c_{\mathrm{M}} = c_0$ at $x = 0$ and $-D_{(\mathrm{m,M})}\frac{\partial c_{\mathrm{M}}}{\partial x} = 0$ at $x = L/2 := \ell$. This latter condition amounts to assuming that the concentration profile is a symmetric function around $x = \ell$. Despite this property is not in general rigorously verified at any instant t, the null-flux condition is computationally convenient, albeit not necessary, and tries to represent the fact that in the bioengineering practice, it is customary to invert the flow direction in order to obtain the most possibly uniform cultivated tissue.

(b) Darcy model for fluid velocity $v_{\mathrm{M}} = v_{\mathrm{M}}(x, t)$ and piezometric head $p_{\mathrm{M}} = p_{\mathrm{M}}(x, t)$:

$$\frac{\partial v_{\mathrm{M}}}{\partial x} = 0, \tag{15a}$$

$$-\frac{\partial p_{\mathrm{M}}}{\partial x} + B_{\mathrm{M}} = 0, \tag{15b}$$

$$B_{\mathrm{M}} = -\frac{\mu_{\mathrm{fl}}\, \Phi_{(\mathrm{m,M})}}{K_{(\mathrm{m,M})}(\Phi_{(\mathrm{m,M})})} v_{\mathrm{M}}, \tag{15c}$$

where $K_{(\mathrm{m,M})}$ is the effective hydraulic permeability, computed as described in Sect. 2.3. The equation system (15) is the 1D homogenized macroscale version of the Navier–Stokes system (2) under the assumption of neglecting inertial terms (see Hsu and Cheng 1990 for a complete derivation). The body force term B_{M} represents the total drag force per unit volume exerted on the perfusion fluid particles by the scaffold/biomass component of the bioreactor. The equation system (15) is supplied by the boundary conditions $p_{\mathrm{M}} = p_0$ at $x = 0$ and $p_{\mathrm{M}} = 0$ at $x = \ell$. The boundary term p_0 is determined by enforcing the global balance

$$-\frac{p_{\mathrm{M}}(\ell) - p_{\mathrm{M}}(0)}{\ell} = \frac{p_0}{\ell} = \frac{\mu_{\mathrm{fl}}\, \Phi_0}{K_{(\mathrm{m,M})}(\Phi_0)} v_{\mathrm{in}}.$$

(c) biomass growth: included through the effective coefficients obtained from Micro- to Macro-scale bridging.

2.3 Micro- to Macro-scale transition

The Micro- to Macro-scale transition gives rise to effective coefficients that keep track, in the homogenized macroscopic model, of the microscale phenomena. Here below we detail the computation of the various coefficients.

2.3.1 Effective porosity

The initial design porosity of the scaffold Φ_0 undergoes significant changes during culture time due to biomass growth. To compute the value of $\Phi_{(\mathrm{m,M})} = \Phi_{(\mathrm{m,M})}(\mathbf{x}_P, t)$ at each time level t and at the centroid of each pore $P \in \mathcal{P}_H$, we refer to the same simplified geometry proposed in Fu et al. (1998), consisting of a cubic hollow box of side $2b$ and cubic hollow portion of side $2a$. The results obtained for this geometry provide a remarkably accurate approximation of the porosity of the cubic pore of Fig. 3b (Fu et al. 1998)

$$\Phi_{(\mathrm{m,M})} = \frac{6(b-a)(2(a-h_{\mathrm{b}}))^2 + (2(a-h_{\mathrm{b}}))^3}{(2b)^3}, \tag{16}$$

where $h_{\mathrm{b}} = h_{\mathrm{b}}(\mathbf{x}_P, t)$ is the biomass thickness predicted from Eq. (12) using the Microscale model in each pore $P \in \mathcal{P}_H$ and a is determined as the only admissible solution of the cubic equation $\zeta^3 - \frac{3}{2}\zeta^2 + \frac{\Phi_0}{2} = 0$, where $\zeta := a/b$, such that $0 \le \zeta \le 1$.

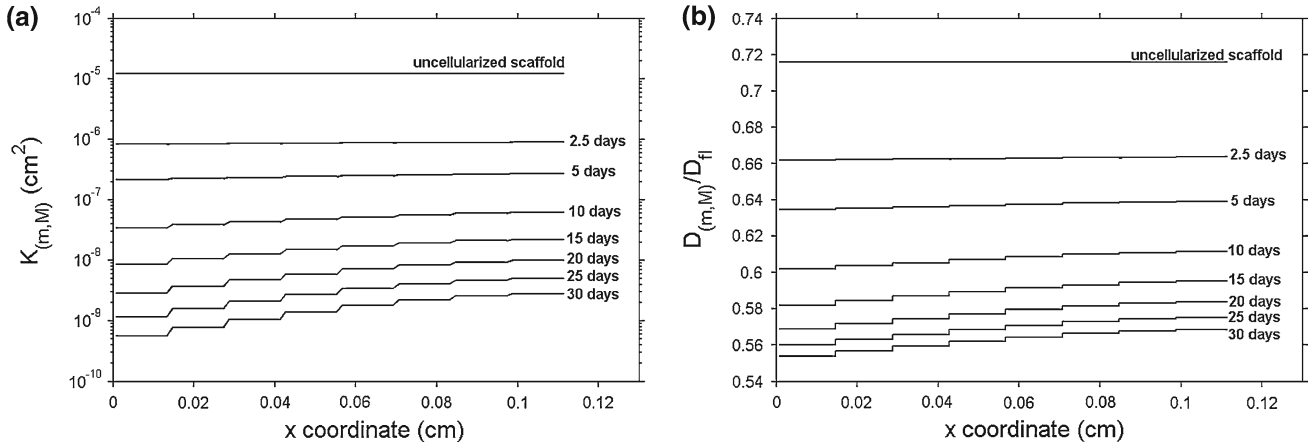

Fig. 4 Effective parameters computed at different culture times for a design porosity $\Phi_0 = 0.8$. **a** Effective permeability computed from Eq. (17). Logarithmic scale is used on the y axis to emphasize the significant variation (two orders of magnitude) of the permeability. **b** Effective diffusivity normalized to clear fluid diffusivity computed from Eq. (18). Notice that even in the uncellularized condition, the obstruction to diffusion exerted by the presence of the scaffold phase causes a reduction of 25 % of the diffusivity. The presence of the growing biomass enhances such a reduction up to 50 %. The reduction is not uniform along the scaffold depth due to the different evolution of biomass growth

2.3.2 *Effective permeability*

The homogenized permeability is computed from the Carman–Kozeny relation (Nield and Bejan 1998) as

$$K_{(\mathrm{m,M})}(\Phi_{(\mathrm{m,M})}) = K_{\mathrm{i}} \frac{\Phi^3_{(\mathrm{m,M})}}{(1-\Phi_{(\mathrm{m,M})})^2}. \tag{17}$$

The intrinsic permeability of the uncellularized scaffold K_{i} is determined by adapting the microscopic theory of dilute random array of spherical particles developed in Hsu and Cheng (1990) to the actual geometry of the scaffold and is given by $K_{\mathrm{i}} = d_K^2/150$, $d_K = 2b\sqrt[3]{6(1-\Phi_0)/\pi}$ being the equivalent particle diameter of the solid fraction of the scaffold pore. The effective permeability resulting from the numerical simulations and obtained using Eq. (17) is shown in Fig. 4a as a function of scaffold depth.

2.3.3 *Effective diffusivity*

Let us denote by $s = s(\mathbf{x}_P, t) = h_{\mathrm{b}}(\mathbf{x}_P, t)/b$ the nondimensional thickness of the biomass layer of pore P. Assuming the scaffold to be impermeable to nutrient diffusion, the following relation is used to compute the homogenized diffusivity $D_{(\mathrm{m,M})} = D_{(\mathrm{m,M})}(\mathbf{x}_P, t)$

$$\begin{aligned}\frac{D_{(\mathrm{m,M})}}{D_{\mathrm{fl}}} &= ((1-\zeta)/((\zeta-s)^2 + s(2\zeta-s)D_{\mathrm{b}}/D_{\mathrm{fl}}) \\ &\quad + (\zeta-s)/((1-(s+1-\zeta)^2)+s(s+2(1-\zeta))D_{\mathrm{b}}/D_{\mathrm{fl}}) \\ &\quad + s/((\zeta-s)+(1-(1-\zeta)^2-(\zeta-s))D_{\mathrm{b}}/D_{\mathrm{fl}}))^{-1}.\end{aligned} \tag{18}$$

The above relation generalizes the ideas of Fu et al. (1998) to the multiphase pore system (scaffold/biomass/fluid). The ratio $D_{(\mathrm{m,M})}/D_{\mathrm{fl}}$ resulting from the numerical simulations and obtained using Eq. (18) is shown in Fig. 4b as a function of scaffold depth.

2.3.4 *Effective consumption rate*

To characterize the effective consumption rate $R_{(\mathrm{m,M})}$, we require that

$$\int_{V_{\mathrm{cub}}} R_{(\mathrm{m,M})}\,\mathrm{d}V = \int_{V_{\mathrm{b}}} R\,\mathrm{d}V.$$

The above bridging condition states that oxygen consumption per unit time referred to the volume of the cubic pore is equal to the consumption per unit time occurring in the biomass layer at the microscopic scale and yields

$$R_{(\mathrm{m,M})} = \frac{\Psi_{\max}\xi_{\mathrm{cells}}V_{\mathrm{b}}(t)}{V_{\mathrm{cub}}} = \frac{\Psi_{\max}N^{\mathrm{tot}}_{\mathrm{cells}}}{V_{\mathrm{cub}}}. \tag{19}$$

2.4 Macro- to Micro-scale transition

The function $c_{(\mathrm{M,m})} = c_{(\mathrm{M,m})}(\mathbf{x}_P, t)$ is defined at each time t as the average macroscopic concentration of each pore $P \in \mathcal{P}_H$ and can be numerically computed using Eq. (25).

2.5 Computational algorithm

We partition the time interval I_t into $N_t \geq 1$ subintervals $I_{t,n} := [t_n, t_{n+1}]$ of uniform width $\Delta t = I_t/N_t$, in such a way that $t_n = t_{\mathrm{start}} + n\Delta t$, $n = 0, \ldots, N_t - 1$. For any function $f = f(\mathbf{x}, t)$, we set $f^n := f(\mathbf{x}, t_n)$. At each time

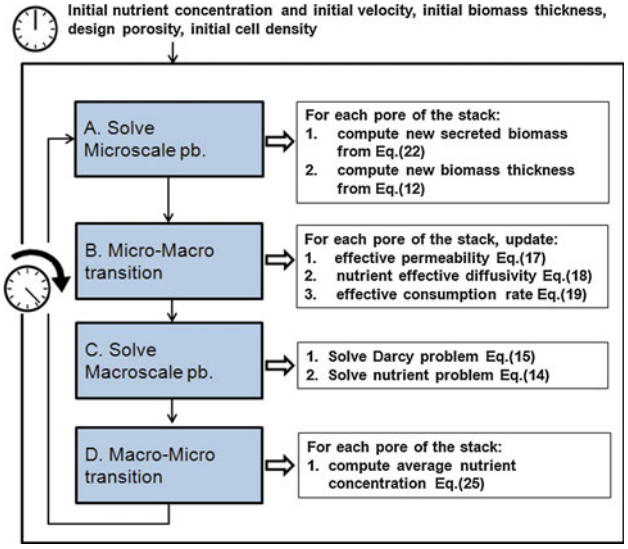

Fig. 5 Staggered algorithm for numerically solving the multiscale model. The initial distribution of nutrient concentration along the scaffold depth is determined by a first run (outside the time loop) of the Macroscale model. Notice that the solution of the Microscale problems at Step A and Scale transition computations at Steps B and D can be carried out in parallel over the stack for each representative pore of the layer. Macroscale computations are serial, but their cost is negligible

level $t_{n+1}, n = 0, \ldots, N_t - 1$, the Microscale and Macroscale problems are solved in sequence in a staggered fashion. Moreover, both the Microscale and Macroscale sub-systems are separately linearized, as detailed in the following sections. The resulting computational algorithm is shown in Fig. 5.

2.5.1 Solution of the Microscale problem at Step A.1

The nutrient problem in Step A.1 is beforehand linearized by replacing in (8a) the consumption term $Q(c_\mathrm{m})$ with $\widetilde{Q}(c_\mathrm{m}) = \chi^n c_\mathrm{m}$, where $\chi^n = -\frac{\Psi_{\max}}{K_{1/2}+c_\mathrm{m}^n}\xi_\mathrm{cells}^n$. At each time level $t_{n+1}, n = 0, \ldots, N_t - 1$, the solution of the linearized Microscale nutrient problem is then the following piecewise smooth function $c_\mathrm{m} : \Omega_{\mathrm{m,fl}}^n \cup \Omega_{\mathrm{m,b}}^n :\to \mathbb{R}$:

$$c_\mathrm{m}^{n+1}(r) = \begin{cases} c_{(\mathrm{M,m})}^n & \text{for } \ r \in (0,\ r_\mathrm{b}^n), \\ \kappa c_{(\mathrm{M,m})}^n \dfrac{F\,(r)}{F\left(r_\mathrm{b}^n\right)} & \text{for } \ r \in (r_\mathrm{b}^n,\ r_\mathrm{w}), \end{cases} \tag{20}$$

where F is the shape function defined as

$$F(r) = \frac{1}{r}\left(\left(r_\mathrm{w}\sqrt{\frac{\chi^n}{D_\mathrm{b}}} + 1\right)\exp\left\{(r - r_\mathrm{w})\sqrt{\frac{\chi^n}{D_\mathrm{b}}}\right\} + \left(r_\mathrm{w}\sqrt{\frac{\chi^n}{D_\mathrm{b}}} - 1\right)\exp\left\{-(r - r_\mathrm{w})\sqrt{\frac{\chi^n}{D_\mathrm{b}}}\right\}\right).$$

Having determined the new biomass position, one can compute the constant α that uniquely specifies the admissible fluid velocity in the spherical pore by enforcing the flux continuity condition (6b), to obtain

$$\alpha^{n+1} = -\kappa D_\mathrm{b}\frac{(r_\mathrm{b}^{n+1})^2}{c_{(\mathrm{M,m})}^n}\frac{F'\left(r_\mathrm{b}^{n+1}\right)}{F\left(r_\mathrm{b}^{n+1}\right)}. \tag{21}$$

2.5.2 Solution of the Microscale problem at Step A.2

We first solve analytically the linearized version of problem (10) obtained by setting

$$\xi_\mathrm{cells} = N_\mathrm{cells}^\mathrm{tot}/V_\mathrm{b}(t_n) := \xi_\mathrm{cells}^n,$$

$$\overline{c}_\mathrm{m} = \int_{r_\mathrm{b}^n}^{r_\mathrm{w}} c_\mathrm{m}^{n+1}(r)\mathrm{d}r/(r_\mathrm{w} - r_\mathrm{b}^n) := \overline{c}_\mathrm{m}^{n+1}$$

to get

$$m_\mathrm{GAG}(t) = m_\mathrm{GAG}^n e^{-K_n(t-t_n)} + m_{\mathrm{GAG,inh}}\left(1 - e^{-K_n(t-t_n)}\right) \qquad t \in [t_n,\ t_{n+1}] \tag{22}$$

where $K_n := (k_\mathrm{GAG}\xi_\mathrm{cells}^n\overline{c}_\mathrm{m}^{n+1})/m_{\mathrm{GAG,inh}}$. This allows us to compute the updated level of secreted biomass $m_\mathrm{GAG}^{n+1} := m_\mathrm{GAG}(t_{n+1})$ and the corresponding new biomass thickness h_b^{n+1} using (12).

2.5.3 Micro-to-Macro transition: Step B

Having computed the new biomass thickness h_b^{n+1}, for each pore of the scaffold matrix, we first compute the new porosity Φ^{n+1} through Eq. (16), and then, we compute the new effective parameters $K_{(\mathrm{m,M})}^{n+1}$ (permeability), $D_{(\mathrm{m,M})}^{n+1}$ (diffusivity) and $R_{(\mathrm{m,M})}^{n+1}$ (consumption rate) using Eqs. (17), (18) and (19), respectively.

2.5.4 Solution of the Macroscale problem at Step C

Let $\mathcal{T}_h$ be a uniform partition of $[0,\ \ell]$ into N_h subintervals T of size $h < H$ and $c_{\mathrm{M},h}$, $J_{\mathrm{M},h}$ be the numerical approximations of c_M and J_M, respectively, with $c_{\mathrm{M},h}$ piecewise linear continuous and $J_{\mathrm{M},h}$ piecewise constant over $\mathcal{T}_h$. At time level t_{n+1}, the first step is to compute the constant value of the Darcy velocity, solution of problem (15)

$$v_\mathrm{M}^{n+1} = v_\mathrm{in}\frac{\mathcal{H}(K(\Phi^{n+1})/\Phi^{n+1})}{K(\Phi_0)/\Phi_0} \quad \text{in} \quad \mathcal{T}_h, \tag{23}$$

$\mathcal{H}(f)$ being the *harmonic average* of the function f over $[0, \ell]$, defined as $\mathcal{H}(f) := (\int_0^\ell f^{-1}(s)\mathrm{d}s/\ell)^{-1}$. Then, the next step consists of solving the nutrient problem (14) using the velocity computed from (23) and using internal fixed point iterations to deal with the non-linear consumption term.

Table 1 Biophysical parameters

Capital letters			Small letters			Greek letters		
Symbol	Value	Units	Symbol	Value	Units	Symbol	Value	Units
D_{b}	2.2×10^{-5}	$\mathrm{cm^2 s^{-1}}$	c_{sat}	6.4×10^{-6}	$\mathrm{g\ cm^{-3}}$	κ	0.5	–
D_{fl}	3.2×10^{-5}	$\mathrm{cm^2\ s^{-1}}$	h_0	5×10^{-4}	cm	μ_{fl}	8.26×10^{-3}	$\mathrm{g\ cm^{-1}\ s^{-1}}$
E	20	–	$k_{\mathrm{GAG,ref}}$	2.38	%ww (day mM (cell/mm^3))$^{-1}$	ρ_{fl}	1	$\mathrm{g\ cm^{-3}}$
$K_{1/2}$	1.92×10^{-7}	$\mathrm{g\ cm^{-3}}$	$m_{\mathrm{GAG,inh}}$	3.5	%ww	Φ_0	0.8	–
$N^{\mathrm{tot}}_{\mathrm{cells}}$	300	–	v_{in}	50×10^{-4}	$\mathrm{cm\ s^{-1}}$	Ψ_{max}	1.28×10^{-16}	$\mathrm{g(cells\ s)^{-1}}$

The Galerkin approximation of (14) with the exponentially fitted finite element method proposed and studied in Brezzi et al. (1989), Gatti et al. (1998) is then carried out. This scheme enjoys several interesting properties. The function $c_{\mathrm{M},h}$ satisfies a discrete maximum principle irrespective of the value of the local Péclet number (Roos et al. 2005). This property prevents the numerical scheme from the onset of spurious oscillations, if the fluid velocity becomes large, and ensures that the discrete Macroscale nutrient concentration is strictly positive and uniformly bounded by c_0. The function $J_{\mathrm{M},h}$ satisfies at each (internal) mesh node x_{i} separating elements T_{i}^- and T_{i}^+ the following discrete conservation law

$$J^+_{\mathrm{M},h} - J^-_{\mathrm{M},h} = \widetilde{Q}_{\mathrm{M}}(c_{M,i})h. \tag{24}$$

Multiplying both sides of (24) by the cross-section pore area in the transverse (y, z) plane, we obtain the "mass flux" equivalent of a Kirchhoff current balance with respect to node x_{i} (see also Wyatt et al. 1980 for a discussion of the electrical analog of reaction–diffusion systems). The average concentration required by Macro- to Micro-scale bridging can be computed as

$$c^{n+1}_{(\mathrm{M,m})}(\mathbf{x}_P) = H^{-1} \sum_{T \in P} \int_T c^{n+1}_{\mathrm{M},h} \mathrm{d}x. \tag{25}$$

3 Results of the simulations

Simulations are carried out using the reference values of the biophysical parameters listed in Table 1 (if not otherwise specified). Adopted values for D_{b}, D_{fl}, c_{sat}, $K_{1/2}$, h_0, $N^{\mathrm{tot}}_{\mathrm{cells}}$, v_{in}, μ_{fl} and Φ_0 are taken from Sacco et al. (2011) and references cited therein. Adopted values for E, $k_{\mathrm{GAG,ref}}$, Ψ_{max} and $m_{\mathrm{GAG,inh}}$ are taken from Nikolaev et al. (2010).

Moreover, we set $N_S = 1{,}000$, $b = 70\ \mu\mathrm{m}$, $N_L = 16$, so that $L = (2b)N_L = 0.224$ cm (cf. Sacco et al. 2011 and references cited therein). We let $[t_{\mathrm{start}}, t_{\mathrm{end}}] = [0, 30]$ days and we use a space discretization parameter in the simulations $h = 1\ \mu\mathrm{m}$ and a time discretization parameter $\Delta t = 1.5$ h.

3.1 The effect of fluid perfusion

We first investigate the oxygen distribution throughout the scaffold thickness for an inlet oxygen tension $p_{\mathrm{O_2}} = 20\,\%$. Figure 6a shows the concentration profiles computed from the Macroscale model as a function of culture time. Each point on the reported curves represents the average concentration in the scaffold at different depths, identified by the layer number, 1 = surface, 8 = center. Results are shown in the static (no perfusion, dotted line) and interstitially perfused ($v_{\mathrm{in}} = 50\ \mu$m/s, solid line) case. Figure 6b shows the biomass thickness in the interstitially perfused regime at different layers, while the difference Δ_h with respect to the biomass thickness in the static case is represented in Fig. 6c. Perfusion yields a higher biomass production, this phenomenon being much more evident for innermost layers, because fluid velocity favorably conveys a larger amount of nutrient to the deepest regions than in static conditions. However, diffusion barriers tend to smooth out the differences for longer culture times, due to the net decrease in permeability (see also Fig. 4b) and—consequently—of fluid velocity magnitude caused by pore obstruction.

3.2 The effect of the inlet oxygen tension

Referring from now on to the perfused case with $v_{\mathrm{in}} = 50\ \mu$m/s, we investigate more in detail the statistical distribution of oxygen tension experienced by cells. The common practice in many bioreactor systems is simply to fix the inlet oxygen concentration at the saturation level c_{sat}. In reality, the situation is more complex, since cartilage cells are in vivo physiologically exposed to lower oxygen levels. Figure 7a–c shows the percentage of cells experiencing a certain range of oxygen tension at time $t = 5, 15, 30$ days parametrized as a function of the inlet concentration (bars represented in different colors). Simulations reveal that different inlet concentrations in the bioreactor result in significantly different distributions of oxygen levels throughout the construct and not only in a shift of the distribution. In particular, an inlet concentration equal to c_{sat} gives rise, as

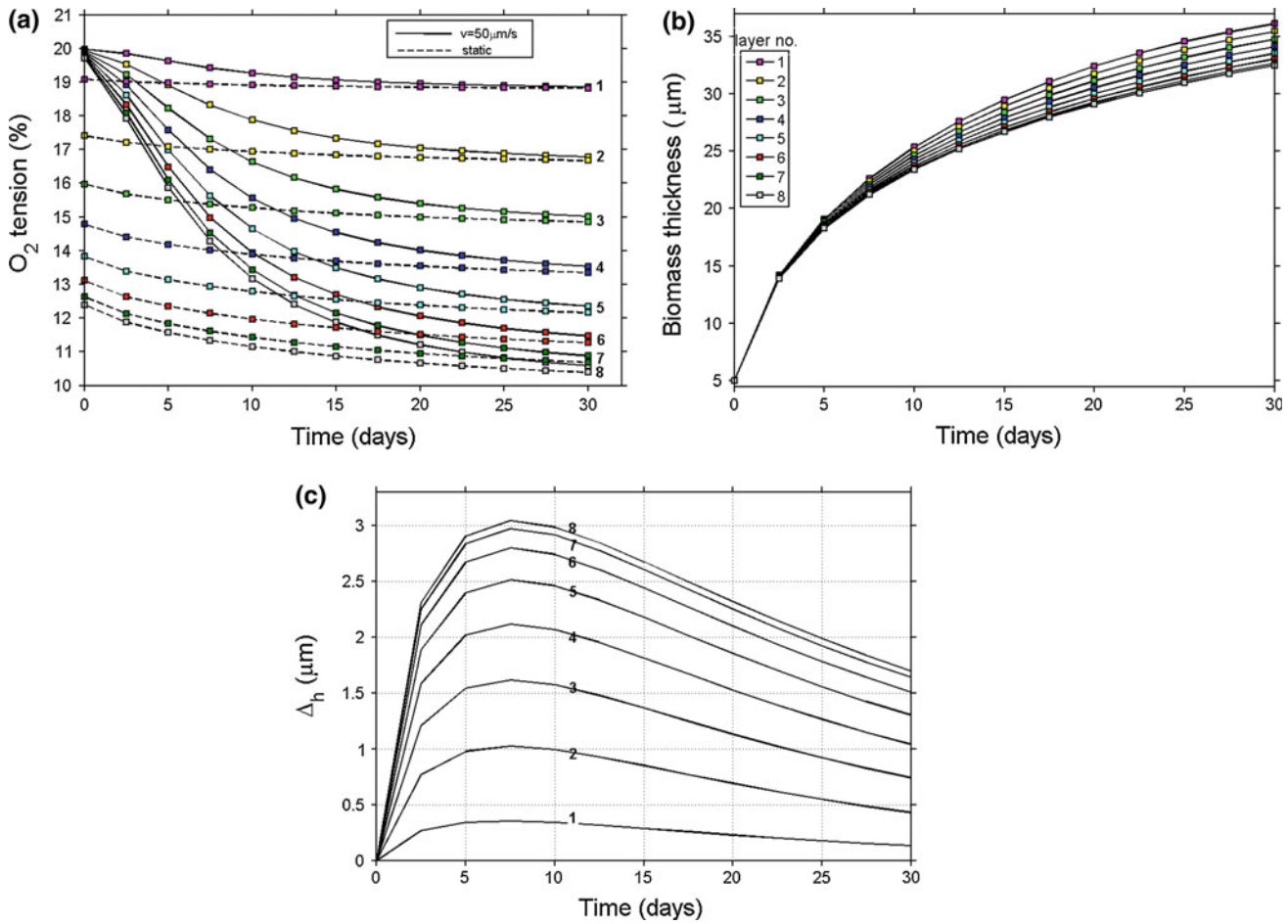

Fig. 6 Effect of fluid perfusion. **a** Macroscale nutrient concentration as a function of time at different scaffold depths (layer 1 = surface, 8 = center of the construct) with $c_0 = c_{\text{sat}}$. *Solid line* $v_{\text{in}} = 50\,\mu\text{ms}^{-1}$, *dashed line* static condition $v_{\text{in}} = 0$, **b** time evolution of biomass thickness under $v_{\text{in}} = 50\,\mu\text{ms}^{-1}$, **c** difference Δ_h between biomass thickness in perfused versus static case parameterized by layer number

culture time advances, to increasingly more non uniform distributions ("flattened bars") of the number of cells receiving a certain level of oxygen, a point which might contrast with the target of obtaining uniform oxygen levels throughout the construct.

3.3 The effect of metabolic parameters and scaffold porosity

Eventually, we use the model to investigate the role of the metabolic regulation parameters and their interplay with scaffold matrix porosity. To this purpose, we first carry out a sensitivity study on effect of the rate of biomass synthesis k_{GAG} (for a fixed porosity $\Phi_0 = 0.8$). Motivated by the experimental analysis carried out in Das et al. (2010) to monitor the effect of oxygen tension in regulating chondrocyte metabolic activity, we assume in this paper a dependence for k_{GAG} on the local oxygen concentration c in the form of a Gaussian distribution $k_{\text{GAG}}(c) = A\text{e}^{-(c-\mu)^2/(2\,\text{std}^2)}$, where $A = k_{\text{GAG,ref}}$ is the maximal amplitude, μ is the average and std the standard deviation (all expressed in oxygen tension units). Different choices of μ and std are considered, in accordance with the indications obtained from the results shown in Fig. 7.

In Fig. 8a, we show the percentage variation of the biomass thickness obtained at $t = 30$ days, to be compared to that obtained using the constant value $k_{\text{GAG,ref}}$, as a function of the layer number (1 = surface, 8 = center of the construct). We see that oxygen variations are more important for the innermost scaffold layers, which attain a lower value of nutrient concentration. More precisely, simulations suggest a scenario for which a metabolic optimization on relatively high oxygen levels ($\mu = 10\,\%$) is disadvantageous, since these levels cannot be attained uniformly in the scaffold due to diffusion barriers. In the case $\mu = 5\,\%$, if a "too narrow metabolic regulation" is displayed by cells (std = 3.125 %), again biomass secretion could be disadvantaged. Then, we discuss the role of the parameter $m_{\text{GAG,inh}}$, which is a lumped

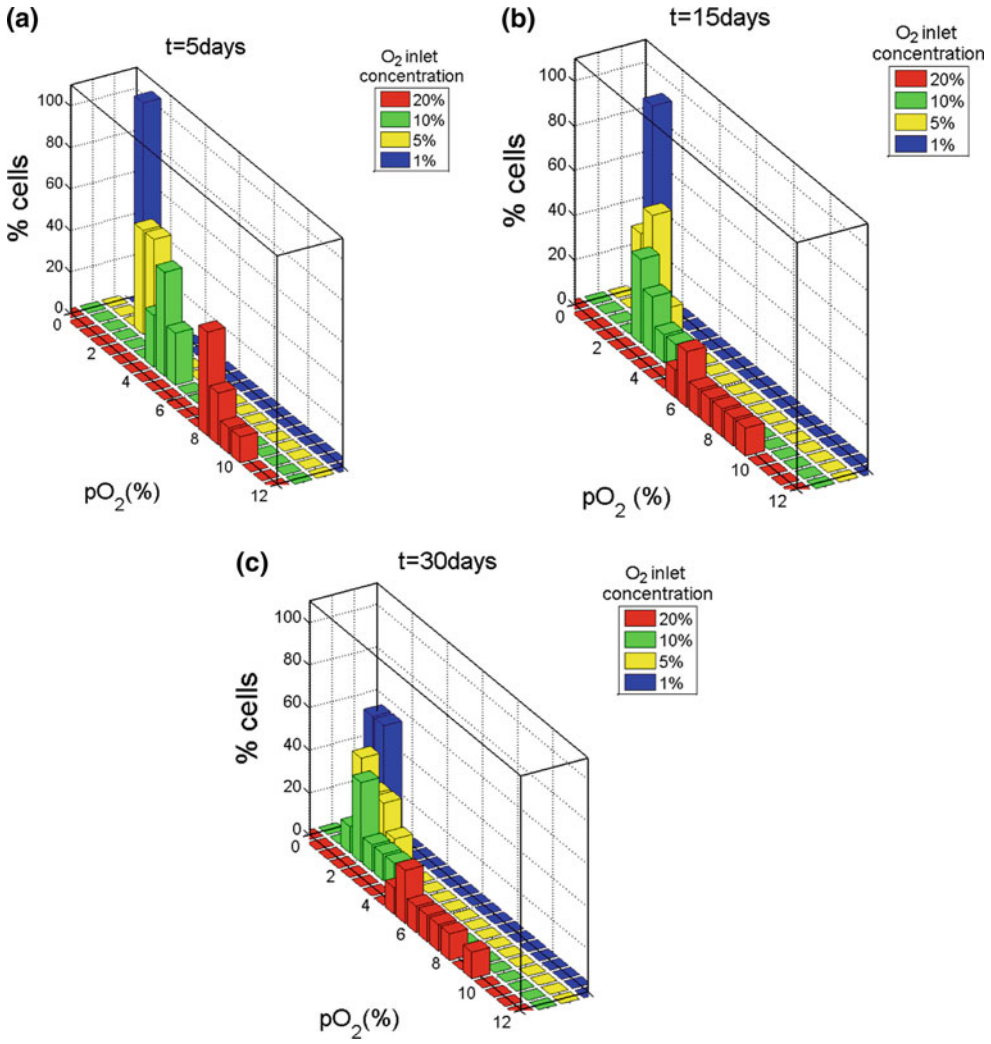

Fig. 7 Percentage of cells in the construct experiencing a certain oxygen tension as a function of the inlet oxygen tensions indicated by *different colors* and corresponding to: 20 % "hyperoxic" condition, 5–10 % "physiological hypoxic" conditions, 1 % "strongly hypoxic" condition, computed at culture times 5, 15, 30 days

representation of biomass production inhibition exerted on cells to maintain a certain homeostatic condition. Beforehand, we need to investigate more thoroughly the relation between biomass thickness, geometry and contact inhibition effects. Relation (13) reveals that for a given pore geometry and cellular post-initial conditions, there exists a threshold value m_{GAG^*} such that if $m_{\mathrm{GAG,inh}} < m_{\mathrm{GAG}^*}$, saturation occurs due to geometrical factors (pore obstruction) irrespective of biophysical homeostatic effects; otherwise, biomass growth is limited by contact inhibition phenomena. These considerations are well represented in Fig. 8b which shows the (theoretical) value of $h_{\mathrm{b,max}}$ obtained from Eq. (13) as a function of $m_{\mathrm{GAG,inh}}$ parametrized on different initial porosities chosen within a physiological interval. The above-mentioned regimes of biomass formation can be clearly distinguished, the threshold value m_{GAG^*} being identified on each curve by the abrupt change of slope. We conclude our simulation analysis by investigating the combined effect of contact inhibition and scaffold porosity on the time evolution of secreted biomass. Figure 8c shows the biomass thickness computed by the multiscale model, as a function of time having set $t_{\mathrm{end}} = 120$ days (steady-state condition). Curves are parametrized for different values of design porosity Φ_0 and different values of $m_{\mathrm{GAG,inh}}$ chosen below and above the threshold value m_{GAG^*}. Computed biomass produced in each layer of the scaffold is shown as a function of time till long culture periods (120 days) for two different values of design scaffold porosity Φ_0 and for the two cases $m_{\mathrm{GAG,inh}} \lessgtr m_{\mathrm{GAG}^*}$. Most superficial layers correspond in all cases to the uppermost curve of each family. Two classes of conclusions can be drawn. First, a higher accumulation of biomass is attained if $m_{\mathrm{GAG,inh}} > m_{\mathrm{GAG}^*}$, for both porosities, even when considering medium to short culture times (blue vs. red or magenta vs. green curves). Second, when the

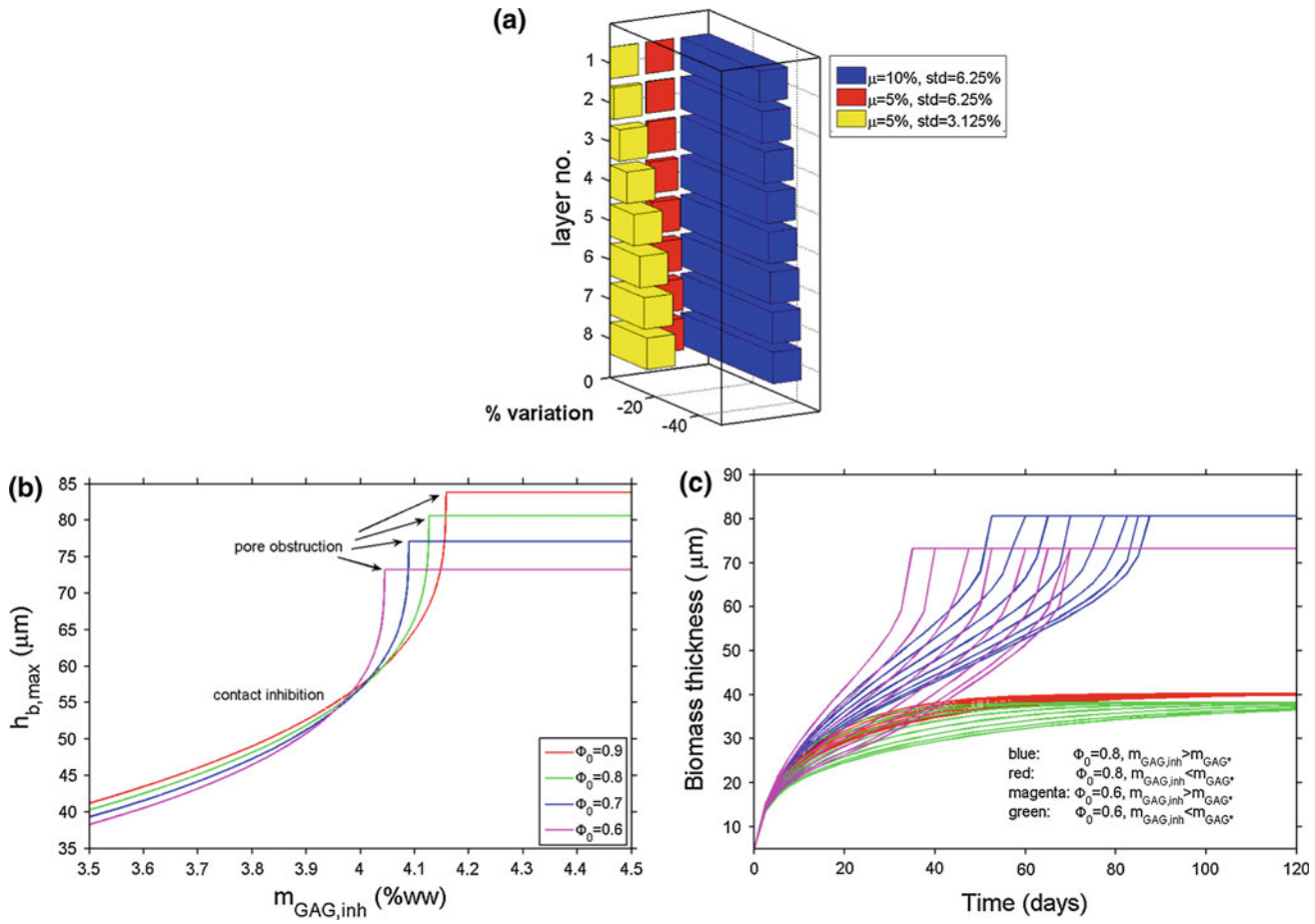

Fig. 8 Sensitivity analysis. **a** Percentage variation of biomass production as a function of the matrix synthesis coefficient k_{GAG} distributed as a random normal variable with respect to results obtained in correspondence of its constant reference value, **b** maximum biomass thickness as a function of the GAG saturation level, **c** combined effect of contact inhibition and scaffold porosity on the time evolution of biomass

driving parameter is design porosity, a higher porosity produces more uniform results along the whole scaffold depth (spread of the curves along the y axis at a given time) due to diffusion barriers exerting a severe influence at later times (blue vs. magenta or red vs. green curves).

4 Discussion

Tissue Engineering is a strategy of regenerative medicine aimed at producing functional substitutes of tissues and organs, starting from donor cells cultivated in a controlled environment (bioreactor) capable of providing adequate conditions for cell viability and metabolism.

A main challenge in bioreactor optimization is the difficulty of establishing a relation between local biochemical and biomechanical processes and design parameters which, properly combined together, lead to achieve specified engineered tissue properties (Freed and Vunjak-Novakovic 2001; Freyria et al. 2005). The usefulness of a more quantitative understanding of the phenomena occurring in bioreactor-based tissue regeneration is thus clear. In this perspective, the interaction with computational models may be profitably exploited to gain information which are often unaccessible to experimental measurements, for example, the effect of a fine tuning of cellular metabolic mechanisms on biomass growth (Knudson and Knudson 1991; Klein and Sah 2007) in conjunction with a given scaffold matrix porosity.

There are numerous computational models of engineered tissue regeneration, based on homogenized averaged approaches (Obradovic et al. 1999; Galban and Locke 1999b; Chung et al. 2007; Sacco et al. 2011; Raimondi et al. 2012) or restricted to small portions of the domain including a selection of biophysical mechanisms with a strong emphasis on CFD (Boschetti et al. 2006; Galbusera et al. 2007; Lesman et al. 2010). The common characteristic of all the above models is that they are restricted on a single scale of the problem.

The model presented in this study is focused on articular cartilage tissue engineered constructs and describes in a

multiscale coupled framework nutrient (oxygen) transport and biomass growth. Despite in Cioffi et al. (2008), an attempt was already made to couple phenomena occurring at different length scales, the model proposed in this article represents, to our knowledge, the first multiscale approach which keeps into account in a self-consistent manner the effect of barrier to the nutrient diffusive process caused by the pore obstruction due to biomass accumulation. This fundamental aspect of the engineered tissue growth process was not covered in Cioffi et al. (2008), because cellular metabolism and consequent production of ECM were not accounted for, thus making the predictions of the proposed Micro- to Macro-scale model significant only for the early stages of the growth process. In this sense, the formulation proposed in the present work provides, in our opinion, a substantial improvement of the multiscale approach of Cioffi et al. (2008).

The mechanism of inter-communication between the two representative scales, Macroscale and Microscale, at which the tissue growth problem is solved in this article, is based on the principle of scale separation and relies on the introduction of suitable scale transition operators (see Lee and Sundararaghavan 2011). Our aim was to obtain a simulation tool able to cover a much wider range of applications and capable of predicting bioreactor performance, even for long culture intervals, requiring at the same time a very limited computational effort. Geometrical simplifications and modeling simplifications allowed us to end up with a first version of such a tool. The validity of such simplifications is, in some cases, biophysically consistent, in others more questionable, and this deserves future investigation. Moreover, in order for the proposed formulation to be employed as a reliable support to the Bioengineer's design activity, an intensive campaign of model validation against experimental data is mandatory. This important and necessary research step might benefit, in a future work, from experimental measurements based on micro–imaging techniques which provide high-resolution time-continuous data (Singh et al. 2005), used in conjunction with novel optically accessible 3D scaffold architectures such as, for example, the miniaturised perfusion chamber (mini-bioreactor) recently presented in Laganà and Raimondi (2011).

Having established that comparison with laboratory results is definitely required for model validation, what kind of biological conclusions can we draw right now from our model to improve bioreactor design?

Biological studies indicate that in vivo cartilage is presumably exposed to "physiologically hypoxic" conditions with an oxygen tension ranging from 10 % in the superficial layers to 1 % in the deepest layers (Grimshaw and Mason 2001; Das et al. 2010). A widespread approach in TE practice is, however, to set a "hyper-physiological" (20 %) oxygen tension at the device inlet, in order to prevent from nutrient shortage in the internal regions of the construct. With the present model, we were able to compute the local distribution of nutrient in the porous scaffold matrix resulting from a certain inlet oxygen tension. For a 20 % inlet oxygen tension, computed oxygen levels (Fig. 6a) encompass a wide spectrum of values throughout the device thickness, ranging from nearly hyper-physiological conditions in the superficial layers to strongly hypoxia in the innermost layers (Freed and Vunjak-Novakovic 2001; Freyria et al. 2005; Devarapalli et al. 2009). We also investigated the spatial dependence of the oxygen distribution as a function of the inlet oxygen tension. Under hyperoxic inlet conditions, the distribution of cell percentage as a function of received oxygen tension is more smoothed out than under hypoxic conditions (Fig. 7). Such a detailed knowledge (in contrast to a simpler read-out approach) of the oxygen tension experienced by cells can be used as a more sophisticated control parameter for cell's metabolism than the sole oxygen inlet tension. This advanced concept is based on the evidence that a certain oxygen tension—which may, but not necessarily, be correspondent to the physiological levels—can be used to finely tune the in vitro synthesis of the various components of the ECM, cell proliferation and differentiation (Das et al. 2010).

Direct perfusion bioreactors have been demonstrated to enhance nutrient convey, while applying hydrodynamic shear to cells, both conditions being believed to favor in vitro chondrogenesis (Cioffi et al. 2008). With the model, we were able to quantify the role of perfusion on the local oxygen distribution in the construct. While the final level of oxygen is strongly influenced by diffusion barriers, the transient behavior to reach steady state is significantly different from static culture conditions (Fig. 6a). As a result, in the same time interval, biomass production is strongly promoted by interstitial flow, this fact being much more evident in the innermost layers (Fig. 6b).

As for the mechanical stimulus exerted on the cells by the fluid-dynamical field, it is known that moderate values of shear stress can enhance ECM production (Raimondi et al. 2006). On the one side, shear stress is not experimentally accessible at the Microscale level, while existing CFD computational models at this scale do not account in a self-consistent manner for the presence of cells (Raimondi et al. 2005). In the model we propose in this article, the shear stress information can be extracted either at the macroscopic level as the Darcy stress or estimated using the Microscopic radial velocity field at the fluid–biomass interface combined with a Coulomb-like friction law to obtain a tangential-like component needed to evaluate the shear stress at the fluid–biomass interface. An extension of this approach to model interstitial fluid flow throughout the growing biomass at the Microscale level is the object of ongoing research activity and will be reported in a subsequent publication.

More in general, we notice that mechanical issues are crucial when describing biomass growth and remodeling.

In this perspective, advanced models of biomass growth incorporating elements of mechanical theory of mixtures to describe the evolving mechanical properties of the tissue during articular cartilage regeneration from explant samples have been proposed, for example, in Klisch et al. (2003), Cowin (2004), Lemon et al. (2006). Such models are sophisticated and promising, but, at the same time, their adoption in the framework of a realistic and quantitative description of the phenomena occurring in a dynamically perfused bioreactor seems to be still a too ambitious goal, especially from the computational point of view.

The regulatory role of biomass production rate is another fundamental biophysical mechanism that we were able to explore. The idea was to test the evolution of biomass growth when not all the cells are subjected to the same "optimal" environmental conditions. Namely, for a given value of scaffold matrix porosity, a Gaussian distribution depending on the nutrient concentration is assumed for k_{GAG} and the resulting biomass thickness at the various scaffold levels is compared to that obtained taking k_{GAG} equal to the constant reference value $k_{\mathrm{GAG,ref}}$ (Fig. 8a). The Gaussian distribution causes in general a reduction in biomass production, due to the fact that oxygen levels in the scaffold vary significantly. More specifically, the reduction is more important when the oxygen tension corresponding to the given central value μ of the Gaussian is experienced by a restricted percentage of cells. A much better performance is achieved when μ is close to a level of oxygenation that is more uniformly represented in the scaffold (case $\mu = 5\,\%$). Notice that this latter value of μ has been selected to reproduce the average oxygen tension experienced by chondrocytes in vivo (Malda et al. 2003). For the same reason, given a certain value of μ, it turns out that tuning metabolic regulation around a narrow range of the concentration parameter (smaller std) is again more disadvantageous in terms of biomass production.

Eventually, reduction of biomass production due to cellular contact inhibition has been investigated in conjunction with different values of scaffold matrix porosity Φ_0, a technologically relevant design parameter (Raimondi et al. 2005; Lesman et al. 2010). The maximum biomass production that can be obtained in a given scaffold pore depends, in a non easily predictable manner, on the interplay between contact effects and available void space. The theoretical results in Fig. 8b indicate that for each considered porosity, the threshold value m_{GAG^*} separates a regime where additional biomass formation is limited by contact effects ($m_{\mathrm{GAG,inh}} \leq m_{\mathrm{GAG}^*}$) from a saturation regime at which biomass production is only determined by pore obstruction ($m_{\mathrm{GAG,inh}} > m_{\mathrm{GAG}^*}$). Figure 8c shows the computed temporal evolution of the biomass thickness in each layer for a very long culture process. Two classes of conclusions can be drawn. First, a higher accumulation of biomass is attained if $m_{\mathrm{GAG,inh}} > m_{\mathrm{GAG}^*}$, for both porosities, even when considering medium to short culture times (blue vs. red or magenta vs. green curves). Second, when the driving parameter is design porosity, a higher porosity produces more uniform results along the whole scaffold depth (spread of the curves along the y axis at a given time) due to diffusion barriers exerting a severe influence at later times (blue vs. magenta or red vs. green curves).

Further aspects of the problem which deserve consideration for future investigation are: (i) the inclusion of more detailed 3D effects while maintaining the computational cost at an affordable level. In this perspective, inhomogeneities in the (y, z) plane can be easily accounted for in our multiscale setting by assuming that the effective parameters are stochastic variables with average value given by the Micro-to-Macro transition proposed in the present model and a certain variability which can be inferred from experimental data; (ii) the inclusion of more detailed models of cell life-cycle, distinguishing between pools of cells in resting, proliferating and secreting states. In this perspective, the change of state of a cell can be monitored via a system of integro-differential equation depending on age maturity parameters (see, e.g., Bernard et al. 2003); (iii) the inclusion of interstitial flow through the growing biomass in the Microscale model by using the same Darcy equations (15) adopted in the Macroscale model for fluid flow. This would allow the calculation of mechanical shear as a function of the radial coordinate in the spherical pore and could be used for future development of a model for the GAG synthesis rate depending on time, position and shear within the biomass; (iv) the inclusion of unbound and degraded GAG fractions in the model for biomass synthesis at the microscale level, to account for degradation of the matrix components due to proteases whose production by chondrocytes and activation may be modulated by a variety of factors (see DiMicco and Sah 2003; Klein and Sah 2007 and references cited therein). More in general, the present Micro- to Macro-scale transition techniques can be extended to other applications in Biology, for example, microcirculation problems where different scales co-exist and computational efficiency is often a major constraint (Secomb et al. 2008).

Acknowledgments This work was partially supported by Politecnico di Milano, under grant 5 per Mille Junior 2009 "Computational Models for Heterogeneous Media. Application to Micro Scale Analysis of Tissue-Engineered Constructs" CUPD41J10000490001 (to P.C. and R.S.).

References

Atala A, Lanza RP, Thomson JA, Nerem R (2011) Principles of regenerative medicine. Academic Press, New York

Bernard S, Pujo-Menjouet L, Mackey MC (2003) Analysis of cell kinetics using a cell division marker: mathematical modeling of experimental data. Biophys J 84(5):3414–3424

Boschetti F, Raimondi MT, Migliavacca F, Dubini G (2006) Prediction of the micro-fluid dynamic environment imposed to three-dimensional engineered cell systems in bioreactors. J Biomech 39(3):418–425

Brezzi F, Marini LD, Pietra P (1989) Two-dimensional exponential fitting and applications to drift-diffusion models. SIAM J Numer Anal 26:1342–1355

Buschmann MD, Gluzband YA, Grodzinsky AJ, Kimura JH, Hunziker EB (1992) Chondrocytes in agarose culture synthesize a mechanically functional extracellular matrix. J Orthop Res 10(6):745–758

Chung CA, Chen CW, Chen CP, Tseng CS (2007) Enhancement of cell growth in tissue-engineering constructs under direct perfusion: modeling and simulation. Biotech Bioeng 97(6):1603–1616

Cioffi M, Kuffer J, Strobel S, Dubini G, Martin I, Wendt D (2008) Computational evaluation of oxygen and shear stress distributions in 3d perfusion culture systems: macro-scale and micro-structured models. J Biomech 41(14):2918–2925

Cowin SC (2004) Tissue growth and remodeling. Ann Rev Biomed Eng 6:77–107

Das RH, van Osch GJ, Kreukniet M, Oostra J, Weinans H, Jahr H (2010) Effects of individual control of ph and hypoxia in chondrocyte culture. J Orthop Res 28(4):537–545

Devarapalli M, Lawrence BJ, Sundararajan VM (2009) Modeling nutrient consumptions in large flow–through bioreactors for tissue engineering. Biotechnol Bioeng 103(5):1003–1015

DiMicco MA, Sah RL (2003) Dependence of cartilage matrix composition on biosynthesis, diffusion, and reaction. Transp Porous Med 50:57–73

Freed LE, Vunjak-Novakovic G (2001) Tissue engineering bioreactors. In: Lanza RP, Langer RS, Vacanti JP (eds) Principles of tissue engineering. Academic Press, San Diego

Freyria AM, Yang Y, Chajra H, Rousseau CF, Ronziere MC, Herbage D, El Haj AJ (2005) Optimization of dynamic culture conditions: effects on biosynthetic activities of chondrocytes grown in collagen sponges. Tissue Eng 11(5–6):674–684

Fu X, Viskanta R, Gore JP (1998) Prediction of effective thermal conductivity of cellular ceramics. Int Commun Heat Mass Transf 25(2):151–160

Galban CJ, Locke BR (1999) Analysis of cell growth kinetics and substrate diffusion in a polymer scaffold. Biotechnol Bioeng 65(2):121–132

Galban CJ, Locke BR (1999) Effects of spatial variation of cells and nutrient product concentrations coupled with product inhibition on cell growth in a polymer scaffold. Biotechnol Bioeng 64(6):633–643

Galbusera F, Cioffi M, Raimondi MT, Pietrabissa R (2007) Computational modelling of combined cell population dynamics and oxygen transport in engineered tissue subject to interstitial perfusion. Comput Methods Biomech Biomed Eng 10(4):279–287

Gatti E, Micheletti S, Sacco R (1998) A new Galerkin framework for the drift-diffusion equation in semiconductors. East-West J Numer Math 6(2):101–135

Grimshaw MJ, Mason RM (2001) Modulation of bovine articular chondrocyte gene expression in vitro by oxygen tension. Osteoarthritis Cartilage 9:357–364

Hsu CT, Cheng P (1990) Thermal dispersion in a porous medium. Int J Heat Mass Transf 33(8):1587–1597

Klein TJ, Sah RL (2007) Modulation of depth-dependent properties in tissue-engineered cartilage with a semi–permeable membrane and perfusion: a continuum model of matrix metabolism and transport. Biomech Model Mechanobiol 6:21–32

Klisch S, Chen SS, Sah RL, Hoger A (2003) A growth mixture theory for cartilage with application to growth-related experiments on cartilage explants. J Biomech Eng 125:169–179

Knudson W, Knudson CB (1991) Assembly of a chondrocyte-like pericellular matrix on non-chondrogenic cells. role of the cell surface hyaluronan receptors in the assembly of a pericellular matrix. J Cell Sci 99(2):227–235

Laganà M, Raimondi MT (2011) A miniaturized, optically accessible bioreactor for systematic 3D tissue engineering research. Biomed Microdev doi:10.1007/s10544-011-9600-0

Landau L, Lifshtiz E (1959) Fluid mechanics. Pergamon Press, Oxford

Langer RS, Vacanti JP (1993) Tissue engineering. Science 260(5110):920–926

Lee S, Sundararaghavan V (2011) Multi-scale modeling of moving interface problems with flux and field jumps: application to oxidative degradation of ceramic matrix composites. Int J Numer Methods Eng 85(6):784–804

Lemon G, King JR, Byrne HM, Jensen OE, Shakesheff KM (2006) Mathematical modelling of engineered tissue growth using a multiphase porous flow mixture theory. J Math Biol 52:571–594

Lesman A, Blinder Y, Levenberg S (2010) Modeling of flow-induced shear stress applied on 3D cellular scaffolds: implications for vascular tissue engineering. Biotechnol Bioeng 105(3):645–654

Malda J, Martens D, Tramper J, Blitterswijk C, van Riesle J (2003) Cartilage tissue engineering: controversy in the effect of oxygen. Crit Rev Biotechnol 23(3):175–194

Martin I, Wendt D, Heberer M (2004) The role of bioreactors in tissue engineering. Trends Biotechnol 22(2):80–86

Nield DA, Bejan A (1998) Convection in porous media. Springer, New York

Nikolaev NI, Obradovic B, Versteeg HK, Lemon G, Williams DJ (2010) A validated model of GAG deposition, cell distribution, and growth of tissue engineered cartilage cultured in a rotating bioreactor. Biotechnol Bioeng 105(4):842–853

Obradovic B, Carrier RL, Vunjak-Novakovic G, Freed LE (1999) Gas exchange is essential for bioreactor cultivation of tissue engineered cartilage. Biotechnol Bioeng 63(2):197–205

Obradovic B, Meldon JH, Freed LE, Vunjak-Novakovic G (2000) Glycosaminoglycan deposition in engineered cartilage: experiments and mathematical model. AIChE J 46:1547–5905

Potter K, Butler JJ, Adams C, Fishbein KW, McFarland EW, Horton WE, Spencer RGS (1998) Cartilage formation in a hollow fiber bioreactor studied by proton magnetic resonance microscopy. Matrix Biol 17(7):513–523

Raimondi MT (2006) Engineered tissue as a model to study cell and tissue function from a biophysical perspective. Curr Drug Discov Technol 3(4):245–268

Raimondi MT, Candiani G, Cabras M, Cioffi M, Laganà K, Moretti M, Pietrabissa R (2008) Engineered cartilage constructs subject to very low regimens of interstitial perfusion. Biorheology 45(3–4):471–479

Raimondi MT, Causin P, Laganà M, Zunino P, Sacco R (2012) Multiphysics computational modeling in cartilage tissue engineering. In: Baumann C (ed) Studies in mechanobiology, tissue engineering and biomaterials, vol 9. Springer, Berlin (in press)

Raimondi MT, Causin P, Mara A, Nava M, Laganà M, Sacco R (2011) Breakthroughs in computational modeling of cartilage regeneration in perfused bioreactors. IEEE Trans Biomed Eng 58(12):3496–3499

Raimondi MT, Moretti M, Cioffi M, Giordano C, Boschetti F, Laganà K, Pietrabissa R (2006) The effect of hydrodynamic shear on 3D engineered chondrocyte systems subject to direct perfusion. Biorheology 43(3–4):215–222

Raimondi MT, Boschetti F, Migliavacca F, Cioffi M, Dubini G (2005) Micro fluid dynamics in three-dimensional engineered cell systems in bioreactors. In: Ashammakhi N, Reis RL (eds) Topics in tissue engineering, vol 2, chap 9, pp 1–26

Roos HG, Stynes M, Tobiska L (1996) Numerical methods for singularly perturbed differential equations. Springer, Berlin Heidelberg

Sacco R, Causin P, Zunino P, Raimondi MT (2011) A multiphysics/multiscale 2D numerical simulation of scaffold-based cartilage

regeneration under interstitial perfusion in a bioreactor. Biomech Model Mechanobiol 10:577–589
Schulz RM, Bader A (2007) Cartilage tissue engineering and bioreactor systems for the cultivation and stimulation of chondrocytes. Eur Biophys J 36:539–568
Secomb TW, Beard DA, Frisbee JC, Smith NP, Pries AR (2008) The role of theoretical modeling in microcirculation research. Microcirculation 15(8):693–698
Singh H, Teoh SH, Low HT, Hutmacher DW (2005) Flow modelling within a scaffold under the influence of uni-axial and bi-axial bioreactor rotation. J Biotechol 119(2):181–196
Vunjak-Novakovic G, Freshney RI (2006) Culture of cells for tissue engineering. Wiley-Liss, New York
Wendt D, Stroebel S, Jacob M, John GT, Martin I (2006) Uniform tissues engineered by seeding and culturing cells in 3D scaffolds under perfusion at defined oxygen tensions. Biorheology 53:481–488
Whitaker S (1999) The method of volume averaging. Theory and application of transport in porous media. Kluwer, Dordrecht, The Netherlands
Williams KA, Saini S, Wick TM (2002) Computational investigation of steady-state momentum and mass transfer in a bioreactor for the production of tissue-engineered cartilage. Biotechnol Prog 18:951–963
Wilson C, Bonassar L, Kohles S (2002) Modelling the dynamic composition of engineered cartilage. Arch Biochem Biophys 408(2):246–254
Wood BD, Quintard M, Whitaker S (2002) Calculation of effective diffusivities for biofilms and tissues. Biotechnol Bioeng 77(5):495–514
Wyatt J, Mikulecky D, DeSimone J (1980) Network modelling of reaction-diffusion systems and their numerical solution using spice. Chem Eng Sci 35(10):2115–2127